Electronic Journal of Biotechnology 57 (2022) 31–41

Contents lists available at ScienceDirect

Electronic Journal of Biotechnology

journal homepage:

Research Article

Effects of *Agaricus blazei* acidic polysaccharide on the aging of mice through keap1-Nrf2/ARE and MAPKs signal pathway

Xiao Guo [a,1], Yujie Ye [a,1], Xinzhu Liu [a], Yu Sheng [a], Ying Yu [b], Yingying Yang [a], Mingliu Gu [a], Rui Lin [a], Baohui Wang [a], Liping An [a,*], Xuechun Lu [c,*]

[a] College of Pharmacy, Beihua University, Jilin, Jilin 132013, China
[b] Department of Cardiovascular Surgery, Second Hospital of Jilin University, Jilin, Jilin 132013, China
[c] Department of Hematology, Nanlou Division & National Clinical Research Center for Geriatric Diseases, Chinese PLA General Hospital, Beijing 100853, China

GRAPHICAL ABSTRACT

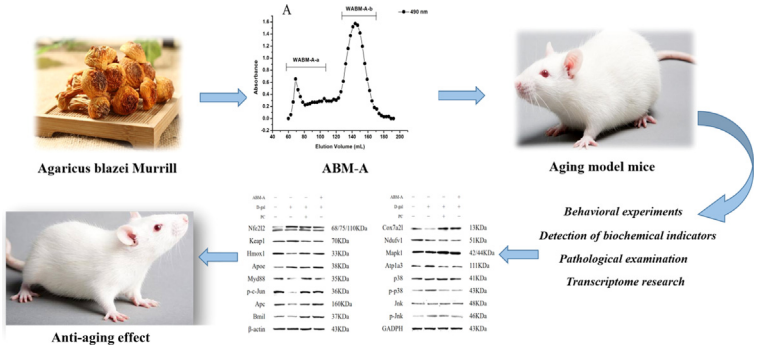

ARTICLE INFO

Article history:
Received 10 May 2021
Accepted 30 March 2022
Available online 05 April 2022

Keywords:
Acidic polysaccharide
Agaricus blazei Murrill
Aging
Anti-aging drugs
Edible fungus
Keap1-Nrf2/ ARE
Learning and memory
MAPKs
Mice

ABSTRACT

Background: In view of the increasing human life and the aging of the population, the search for safe anti-aging drugs has become a hot topic. *Agaricus blazei* Murrill is a rare edible fungus, with a variety of biological activities. The purpose of this study was to clarify the anti-aging effect and mechanism of ABM-A on the aging induced by D-Galactose in mice.

Results: The result showed that ABM-A contained 87.2% of glucose, 3.3% of galactose, 3.8% mannose and 5.7% gluconic acid. The behavior of mice in the treatment group was significantly improved after administration of ABM-A. And the activity of SOD and CAT and the level of T-AOC were increased ($p < 0.05$), the content of MDA and ROS was decreased ($p < 0.05$) in the serum of mice in ABM-A group. The results of mechanism research showed that nine genes were screened out by functional annotation and enrichment analysis for the verification by RT-qPCR, and the results of RT-qPCR were consistent with those of RNA-seq. Western Blot results showed that ABM-A upregulated the expression of Hmox1, Myd88, p-c-Jun, Apc, Bmil, Cox7a2l and Ndufv1, down-regulated the expression of Nfe2l2, Keap1, Apoe, Mapk1and Atp1a3, and decreased the phosphorylation of p38 and Jnk, suggesting that it may play an anti-aging effect by regulating Nrf2/ARE and MAPKs superfamily signal pathways.

Peer review under responsibility of Pontificia Universidad Católica de Valparaíso

* Corresponding authors.
E-mail addresses: lpan@beihua.edu.cn (L. An), luxuechun1970@163.com (X. Lu).
[1] These authors contributed equally to the work.

https://doi.org/10.1016/j.ejbt.2022.03.004

Conclusions: ABM-A can reduce oxidation reaction and play an anti-aging role through Keap1-Nrf2/ARE and MAPKs signaling pathway.

How to cite: Guo, X, Ye Y, Liu X, et al. Effects of *Agaricus blazei* acidic polysaccharide on the aging of mice through keap1-Nrf2/ARE and MAPKs signal pathway. Electron J Biotechnol 2022;57. https://doi.org/10.1016/j.ejbt.2022.03.004

1. Introduction

In the past century, the decline in cognitive ability has become one of the greatest health threats to the elderly [1]. The aging is the last stage of life, and with the occurrence of aging, the morphological and structural deterioration and functional decline may occur in tissues and organs of the body [2]. In recent years, many aging-related mechanisms are proposed, such as the telomere theory, the immune function degradation theory, the DNA damage repair theory, the neurotransmitter theory, the free radical theory, the cell apoptosis theory, the non-enzymatic glycosylation aging theory and the metabolic imbalance theory of aging [3,4,5,6], of which the free radical theory believes that severe pathological changes may occur when free radicals are excessively produced or the human body's capacity to scavenge them is reduced, so the scavenging of the excess reactive oxygen free radicals has an important physiological significance [7,8], and the research and development of safe and effective natural anti-aging medicines has become the focus of attention.

Agaricus blazei Murrill (*Agaricus blazei*, *Agaricus*), also known as Brazilian mushroom, is a fungus of *Agaricus campestris* (*Stropharia*) genus, *Agaricaceae* (*umbelliferae*), *Agaricase*, *Hymenomycetes*, *Basidiomycotina* native to coastal rainforests in Brazil, southern North America and Peru, not only a popular food in the local area, but also used in cancers, infections and other diseases [9,10,11]. Studies have shown that *Agaricus blazei* Murrill polysaccharide has the effect of anti-tumor, regulation of immunity, improvement of lipid level and protection of damaged nerve [12,13,14]. Our previous study showed that *Agaricus blazei* Murrill polysaccharide had an obvious antioxidant activity and could scavenge free radicals in vitro, but its anti-aging effect and mechanism were not clear.

In this study, an *Agaricus blazei Murrill* acidic polysaccharide (ABM-A) was isolated and purified, an aging model induced by D-galactose (D-gal) was established for the observation on the anti-aging effect of ABM-A, and the differentially expressed genes among aging mice treated with ABM-A were analyzed in transcriptology for investigating the molecular mechanism of anti-aging effect of ABM-A, in order to find the effective way of ABM-A to delay aging, which may provide a theoretical basis for the development and utilization of *Agaricus blazei* Murrill.

2. Materials and methods

2.1. ABM-A preparation

The *Agaricus blazei* that had been dried to the constant weight was soaked at a water-to-material ratio of 20:1 overnight and extracted 3 times at 100°C for 3 h. The extracted solution was concentrated and centrifuged at 4500 rpm for 10 min to obtain the supernatant, the supernatant was precipitated with 80% ethanol, left standing overnight, and then centrifuged at 4500 rpm for 10 min again and the sediment was collected. The sediment was washed with 95% ethanol and absolute ethanol in turn, and dried routinely to obtain a crude water-extracted ABM polysaccharide. The crude water-extracted ABM polysaccharide was dialyzed in a dialysis bag and freeze-dried to obtain the total *Agaricus blazei* polysaccharide (ABM). The ABM was loaded on an balanced DEAE-cellulose column (7.5 × 30 cm, Cl-type) for the fraction, eluted with 0.5 M NaCl, desalted with the hollow fiber with a molecular weight cutoff of 3000 Da and freeze-dried to obtain the fraction A, namely ABM-A. The monosaccharide composition in ABM-A samples was determined according to the retention time of the chromatographic peaks of monosaccharide standard and mixed standard samples by Shimadzu HPLC system. ABM-A obtained by the elution with 0.5 M NaCl was further separated and purified by Sepharose Cl-6B chromatography column (2.6 × 100 cm), in which the eluant was 0.15 M NaCl solution, the elution flow rate was 0.4 mL/min, and 8 ml was collected from each tube (20 min/tube). All the fractions were monitored with the phenol–sulfuric acid method at 490 nm. The distribution of total sugar was determined by phenol–sulfuric acid method, the appropriate elution peak was collected according to the absorbance elution curve, the dialysis bag with 3500 Da molecular weight cut-off was used to dialyze the eluate for its desalting, and the desalted eluate was concentrated and frozen dry to obtain the main polysaccharide component. High performance gel performance chromatography (HPGPC) was used to determine the molecular weight.

2.2. The effect of ABM-A on the learning and memory of D-gal-induced aging mice

2.2.1. Grouping and administration

Seven-week-old male ICR mice weighing 20–24.5 g were obtained from Changchun Yisi experimental animal Co., Ltd (Changchun, China). ICR mice were randomly divided into 4 groups, 18 mice in each group, and administered successively for 10 weeks. (1) Blank control group (CON group): the mice were intragastrically given distilled water and subcutaneously injected with normal saline at the back of their neck; (2) Model group (MOD group): the mice were intragastrically given distilled water and subcutaneously injected with 200 mg/kg D-gal at the back of their neck; (3) Positive control group (PC group): the mice were intragastrically given 800 mg/kg piracetam and subcutaneously injected with 200 mg/kg D-gal at the back of their neck; (4) ABM-A group: the mice were intrgastrically given 800 mg/kg ABM-A and subcutaneously injected with 200 mg/kg D-gal at the back of their neck.

2.2.2. Behavioral experiments

On the 9th week of administration, the step-through test was carried out. 36 V 50 Hz alternating current was connected to the electric grid at the bottom of dark avoidance instrument, and then the mice were first trained in the instrument for 3 min. At the beginning of the training, the mouse were put into the light chamber to face to the hole between the two chambers, and the number of times the mice entered the dark chamber and the time when they entered the dark chamber for the first time within 5 min were recorded, that is, the number of errors and the latency, respectively. The test began after an interval of 24 h.

After the end of the step-through test, the step-down test was carried out using a mouse step-down apparatus. At the beginning

of the training, the mice escaped to the safety platform after an electric shock, and then stepped down from the platform, in which when the both feet of mice touched the electric grid to be shocked was considered a wrong response (the number of errors), and the latency and the number of errors within 3 min were recorded. The test was repeated once more 24 h later. The latency and the number of errors of mice in the training and repeated test was used to examine the learning and memory ability of mice.

After the step-down test, the Morris water maze orientation navigation test was carried out. Firstly, the mice were put into the pool facing to the pool wall in the three quadrants except the quadrant where the platform was located, and the test time was set at 120 s, in which the time from entering the water to finding the platform for the mice was recorded as the escape incubation period (latency). If the mice found the platform within 120 s, they were allowed to stay on the platform for 10 s, and if they could not find the platform within 120 s, they were guided to the platform and allowed to stay on it for l0 s, and the latency was recorded as 120 s. The orientation navigation test lasted for 6 d. On the 7th day, the spatial probe test was performed, in which the platform was removed, and the mice were put into the pool from the second quadrant for 120 s, and the residence time of mice in the third quadrant, the percentage of distance to the third quadrant, the time of first crossing the place where the platform had been placed and the number of crossing the place were recorded.

2.2.3. Detection of biochemical indicators in the serum and brain tissue

After the end of the mouse behavioral experiments, the body weight of each mouse was accurately weighed and recorded. The blood samples of mice were collected by removing their eyeballs. After left standing for 10 min, the blood was centrifuged at 3500 rpm for 10 min, and then the serum was taken for use. The mice were sacrificed, and their whole brain tissues were taken out quickly on an ice platform, repeatedly washed with pre-cooled normal saline, dried with a piece of filter paper, and the weight of the whole brain was weighed by an electronic balance.

The brain tissue homogenate was centrifuged at 3000 rpm and 4°C for 15 min to obtain the supernatant, namely 10% brain homogenate. The activity of SOD and CAT, the level of T-AOC and the content of MDA and ROS in the serum of mice were determined strictly according to the instructions of the kits.

2.2.4. Pathological examination of brain tissue

HE staining. The hippocampal tissue was fixed at 4°C for 24 h with 4% paraformaldehyde, then washed 3 times with PBS solution, dehydrated with 30%, 50% and 70% ethanol gradient, respectively, 10 min for each gradient, paraffin-embedded, and sliced. The paraffin-embedded slices were stained with HE, according to the instructions of HE staining, and the sections were observed under a light microscope for examining the pathological changes of brain tissues.

Immunofluorescence double labeling staining. The mice were intraperitoneally injected with 20% bromodeoxyuridine (BrdU) on the last 5 d of modeling. The brain tissues were taken after the ventricular perfusion and dehydrated with 4% paraformaldehyde, 20% sucrose solution, 30% sucrose solution in turn, quickly frozen with liquid nitrogen, and embedded to make frozen slices. The slices were soaked in 0.1 mol·L^{-1} PBS and rinsed, boiled in 0.01 M citric acid buffer (pH = 6.0) for 5 min, cooled to room temperature, soaked in PBS solution and rinsed, and added with 0.3% Triton X-100 and left standing at room temperature for 5 min. 10% BSA/PBS-T (0.05% NaN3) solution was dropped on the slices for 1.5 h and then the first antibody Anti-NeuN (1:500) rabbit Anti-BrdU (1:200) mouse was dropped on them, incubated at 4°C overnight. The first antibody was sucked out, the mixed secondary antibody containing 1:1000 Anti-mouse IgG-Alexa Fluor 488 and 1:1500 Anti-Rat IgG-Alexa Fluor 594 was added on them, and kept in dark place at 4°C overnight. The second antibody was sucked out, then washed with PBS three times, Hoechst 33258 dye solution was added on the slices, and the slices were kept at room temperature for 30 min. The slices were washed three times with PBS solution and mounted with the neutral balsam, and then the sections were examined under a laser confocal fluorescence microscope.

2.3. Study on the mechanism of effect of ABM-A on learning and memory of D-Gal-induced aging mice

2.3.1. Preparation of the total RNA of brain tissues

The total RNA was extracted from the hippocampus tissue of mouse. The RNA OD values were measured at 260 nm and 280 nm wavelength by an ultra-micro nucleic acid protein analyzer (scandrop 100), respectively. The purity standards of the sample were OD260/OD280 = 2.1–2.2. Agarose gel electrophoresis was used to detect the integrity of total RNA.

2.3.2. Establishment of sequencing library

After the quality inspection verified the total RNA, the eukaryotic mRNA enriched by magnetic beads connected with Oligo (dT) was used. The extracted mRNA was randomly interrupted into short fragments by fragmentation buffer. The segmented mRNA was used as the template, a single-stranded cDNA was synthesized with six-base random hexamers, and then the buffer, dNTPs, RNaseH and DNA Polymerase I were added to it for the synthesis of double-stranded cDNA. The double-stranded products were purified with AM Pure XP beads, the viscous end of DNA was repaired to a flat end by utilizing the activities of T4 DNA polymerase and Klenow DNA polymerase, and base A was added to the 3′ end of DNA. After the selection of segments by AM Pure XP beads, the final sequencing library was obtained by PCR amplification. After the quality inspection confirmed the library, Illumina Hiseq 4000 was used for sequencing, and the sequencing read-length was double-terminal 2*150 bp (PE150).

2.3.3. Analysis of transcriptomic data

The original data obtained by sequencing were mapped to the mouse genome using TopHat 2.1.0 software. Cufflinks was used to evaluate the gene expression values and normalize them. The protein-coding genes beginning with "NM" were selected, and FPKM (fragments per kilobase per million mapped reads) was introduced to calculate the expression level of genes. The differentially expressed genes were screened according to the criteria of FPKM > 10, pval < 0.05, fc > 1.5 and fc < 0.6. The names of annotated proteins and their genes were determined according to the GeneID of differentially expressed genes and the location of TranscriptID in the result table of protein annotation, and the cellular composition, molecular function and biological process of differentially expressed genes were analyzed in bioinformatics by gene ontology (GO) classification and KEGG Pathway.

2.3.4. Differential gene mRNA expression verified by qRT-PCR

The names of differentially expressed genes and related proteins were screened, and the differentially expressed genes related to aging were selected and verified. The samples used in this verification test were the same as those used in the sequencing of transcriptome. The reverse transcription for the cDNA synthesis of RNA was carried out by using TUREscript 1st Stand cDNA SYNTHESIS Kit (Aidlab Company, Beijing, China). The sequences of primers are shown in Table 1.

2.3.5. Expression of differential gene proteins verified by Western Blot

The proteins of the hippocampus of the mouse were extracted and separated by 12% SDS-PAGE gel electrophoresis, and then

Table 1
Primer sequences used for qRT-PCR.

Primers	Tm (°C)	Forward direction	Reverse direction
GAPDH	58	GGTGAAGGTCGGTGTGAACG	CTCGCTCCTGGAAGATGGTG
Cox7a2l	58	AGCGGACAGGTGGTGAAGT	AAACCAACTGCCCACAAATAGAGG
Taok3	58	TAGAGTTGGCGGAGCGGAAG	GGAGTCATTCTGAGCGATGTGGTA
Atp1a3	58	CAGTCATCTTCCTCATCGGCATCA	TTGGCGGTCAGCGTCAGA
Gabra1	58	CCAGAGCAGAGCAGAGTATTCAG	TCTTTGGACCTTCTTACCCTCTCT
Apc	58	GGAATGGTGAGTGGCATCATAAGC	CTGTCTGTGGAGGAGGTGGAG
Bmi1	58	GGACTGACGAATGCTGGAGAG	AGGAAGAGGTGGAGGGAACA
Apoe	58	ACCGCTTCTGGGATTACCT	GTGCCGTCAGTTCTTGTGT
Ank3	58	GCCGCCACAAAGAAAGGAAACAC	CGTTGACATTCGCTCCGTTCGTA
Ndufv1	58	AGAGACGGCACTTATTGAATCCA	GCATCCAAACACTCCCACATC

transferred onto the polypropylidenfluoride (PVDF) membranes treated with methanol. The membranes were placed in a oscillating table and blocked with the TBS-T blocking solution containing 5% skimmed milk powder for 1 hour, and then the first antibodies of β-actin (1:50000) and GAPDH (1: 2000), Nfe2l2 (1:500), Keap1 (1:500), Hmox1 (1:500), Apoe (1:1000), Myd88 (1:500), p-c-Jun (1:500), Apc (1:500), Bmil (1:2000), Cox7a2l (1:100), Ndufvl (1:100), Mapk1 (1:500), Atpla3 (1:200), Mapk14 (p38) (1:500), p-p38 (1:1000), Mapk8 (Jnk) (1:500) and p-Jnk (1:2000) were added onto the membranes, incubated at room temperature for 2 h. All the antibodies used were purchased from ABclonalTechnology. The membranes were washed 5 times with TBS-T, 15 min each time, then the second antibodies (1:2000) were added onto the membranes, incubated at room temperature for 1 h, washed 5 times with TBS-T again, 15 min for each time, and finally ECL chromogenic solution was added onto the membranes for the color development.

2.4. Statistical analysis

The experimental data were expressed by mean ± *SD*, the statistical data were analyzed using SPSS 17.0, and the charts were processed using GraphPad Prism 7.0. $p < 0.05$ when the difference was significant. $p < 0.01$ when the difference was very significant.

3. Results

3.1. ABM-A preparation

The ash was removed by a 1000 Da dialysis bag to obtain *Agaricus blazei* polysaccharide (ABM), and ABM was loaded on a DEAE-cellulose column for ion exchange chromatography and eluted with 0.5 M NaCl to obtain the acidic fraction ABM-A. The yield of ABM was 4.7%, and the total sugar content of ABM was 75.1%, the uronic acid content 1.9% and the protein content 5.6%, respectively; the yield of ABM-A was 47.5%, and the total sugar content of ABM-A was 74.1% and the uronic acid content 8.2% (Table 2). The monosaccharide composition of ABM was 79.1% Glc, 12.4% Gal, 4.5% Man, 1.3% Fuc, and 2.7% GLcA. The monosaccharide composition of ABM-A was 87.2% Glc, 3.3% Gal, 3.8% Man, and GlcA 5.7% (Table 3). ABM-A was further graded by Sepharose-CL-6B to get two obvious elution peaks, and after being collected and lyophilized, two fractions ABM-A-a and ABM-A-b were obtained, as shown in Fig. 1A. The homogeneity of fraction polysaccharides was determined by HPGPC. The results showed that the molecular weight of ABM-A-a was about 360 KD and the molecular weight of ABM-A-b was about 10 KD. The results are shown in Fig. 1B and C.

3.2. Effects of ABM-A on the learning and memory of D-gal-induced aging mice

3.2.1. Effects of ABM-A on the learning and memory of D-gal-induced aging mice (Behavioral experiments)

The step-through test showed that compared with that in CON group, the latency was significantly shortened and the number of errors was significantly increased in MOD group ($p < 0.05$), and compared with that in MOD group, the latency was significantly prolonged and the number of errors was significantly decreased in ABM-A group ($p < 0.05$), as shown in Fig. 2A and B.

The step-down test showed that compared with that in CON group, the latency was significantly prolonged and the number of errors was significantly increased in MOD group ($p < 0.05$), and compared with that in MOD group, the latency was significantly shortened and the number of errors was significantly decreased in ABM-A group ($p < 0.05$), as shown in Fig. 2C and D.

The results of Morris water maze test showed that the escape latency of mice in the different groups decreased with the increase of training time ($p < 0.05$), and the decreased latency was largest in CON group and smallest in MOD group. From the second day to the 6th day, compared with that in CON group, the latency in MOD group was significantly prolonged, and compared with that in MOD group, the latency in ABM-A group was significantly shortened ($p < 0.05$), as shown in Fig. 2E. In the spatial probe test, compared with that in CON group, the time of finding the platform (latency) was significantly prolonged and the number of crossing the place where the platform had been placed was significantly decreased in MOD group, and compared with that in MOD group ($p < 0.05$), the time of finding the platform (latency) was significantly shortened and the number of crossing the place where the platform had been placed was significantly increased in ABM-A group ($p < 0.05$) (Fig. 2F and G).

3.2.2. Effects of ABM-A on biochemical indicators in D-gal-induced aging mice

As shown in Fig. 3, compared with those in CON group, the SOD and CAT activities and T-AOC levels were decreased ($p < 0.05$), and the ROS and MDA contents were increased ($p < 0.05$) in the serum of mice in MOD group significantly; compared with those in MOD

Table 2
Composition analysis of ABM and ABM-A.

Polysaccharide	Yield (%)	Total sugar (%)	Uronic acid (%)	Protein (%)	Ash (%)
ABM	4.7	75.1	1.9	5.6	5.1
ABM-A	47.5	74.1	8.2	4.8	5.1

Table 3
Monosaccharide composition of ABM and ABM-A.

Polysaccharide	Monosaccharide composition (Mol%)				
	Glc	Gal	Man	Fuc	GlcA
ABM	79.1	12.4	4.5	1.3	2.7
ABM-A	87.2	3.3	3.8	–	5.7

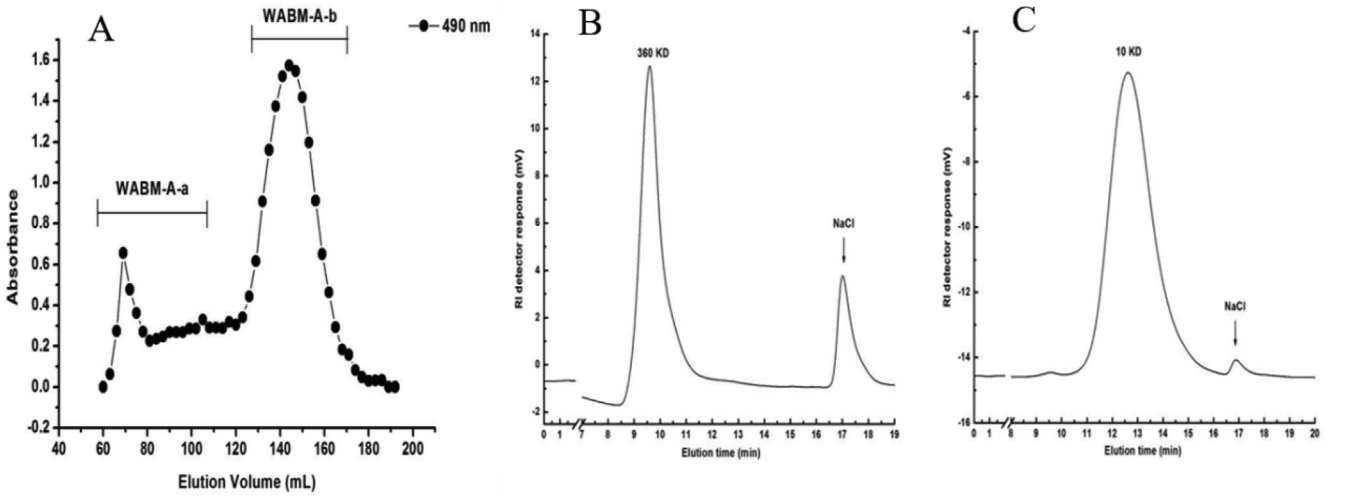

Fig. 1. Eluting curve of WABM-A. (A) Gel chromatography, (B) WABM-A-a on HPGPC, (C) WABM-A-b on HPGPC.

group, the SOD activities and T-AOC levels ($p < 0.05$), and the CAT activities ($p < 0.01$) were increased, and the ROS ($p < 0.05$) and MDA ($p < 0.01$) contents were decreased, in the serum of mice in ABM-A group significantly.

3.2.3. Effects of ABM-A on pathological changes of the hippocampal tissue of D-gal-induced aging mice

The HE staining showed that the neurons were closely arranged, the layers of neurons were clear, the size of neurons was uniform, the morphological structure of neurons was intact, and the boundary was clear, with plenty of cytoplasm in the hippocampus of mice in CON group. The hippocampal tissue of mice in MOD group showed the typical neuropathological changes, enlarged intercellular space, disordered and loose arrangement of cells, unclear layers, decreased number of cells, and irregular shape of some hippocampal cells. In PC and ABM-A groups, the number of cells were significantly increased, the arrangement of neurons was close and orderly, the layers of neurons were clear, and the shape and volume of neurons were normal. The results are shown in Fig. 4A.

The immunofluorescence double labeling staining showed that Brdu/Neu N double labeled positive cells were mainly distributed in the granular cell layer, and a few in the portal area, showing a single or two and no cluster in the hippocampus of mice in CON group; Compared with that in CON group, the number of Brdu/Neu N double labeled positive cells was significantly lower in the hippocampus of mice in MOD group ($p < 0.01$); Compared with that in MOD group, the number of Brdu/Neu N double labeled positive cells was significantly higher in PC and ABM-A groups ($p < 0.05$) (Fig. 4B and C).

3.3. Results of study on the mechanism of effect of ABM-A on the learning and memory of D-gal-induced aging mice

3.3.1. Results of total RNA quality control

The RNA of the hippocampus of mice was detected by using an ultramicro nucleic acid protein tester. A260/A280 values of RNA in all groups were between 2.00 and 2.20, and the concentrations were equal to or more than 50 ng/μL, indicating that all the conditions met the requirements for transcriptome sequencing.

3.3.2. Results of transcriptomic analysis

Sequencing and pre-treatment: The results of RNA-seq data control showed that Clean Reads of 52009586, 45348742, 49179206, 47162910, 42740450 and 38538398 BP were obtained by filtration, and the effective rate was more than 97%, Q20 and Q30% were more than 96%, and GC contents were between 48% and 50%, indicating that the overall quality of the transcriptome data were good, and the downstream analysis could be carried out, as shown in Table 4.

Functional annotation: Hisat was used to align the pretreated valid data (Valid Data) with those of the reference genome, a total of 34,770 genes were identified in the hippocampal tissue of mice, and the GO functional annotation showed that a total of 922 unigenes were clustered to be involved in the 50 functional categories of biological process, cellular component and molecular function, including secretory granule, response to nicotine, response to morphine, positive regulation of renal sodium excretion, positive regulation of neuroblast proliferation, positive regulation of cytosolic calcium ion concentration, peptide antigen binding, neuropeptide hormone activity, neurohypophyseal hormone activity, MHC class II protein complex, MHC class I protein complex, maternal aggressive behavior, insulin receptor binding, hyperosmotic salinity response, grooming behavior, β-2-microglobulin binding, axon terminus, antigen processing and presentation of peptide or polysaccharide antigen via MHC class II, antigen processing and presentation of peptide antigen via MHC class I, and antigen processing and presentation, totally 20 GO Term, as shown in Fig. 5A and B. The results of the KEGG pathway enrichment analysis showed that a total of 43 differentially expressed genes were assigned to 95 metabolic pathways, and more genes were involved in Neuroactive ligand-receptor interaction, Cell adhesion mole-

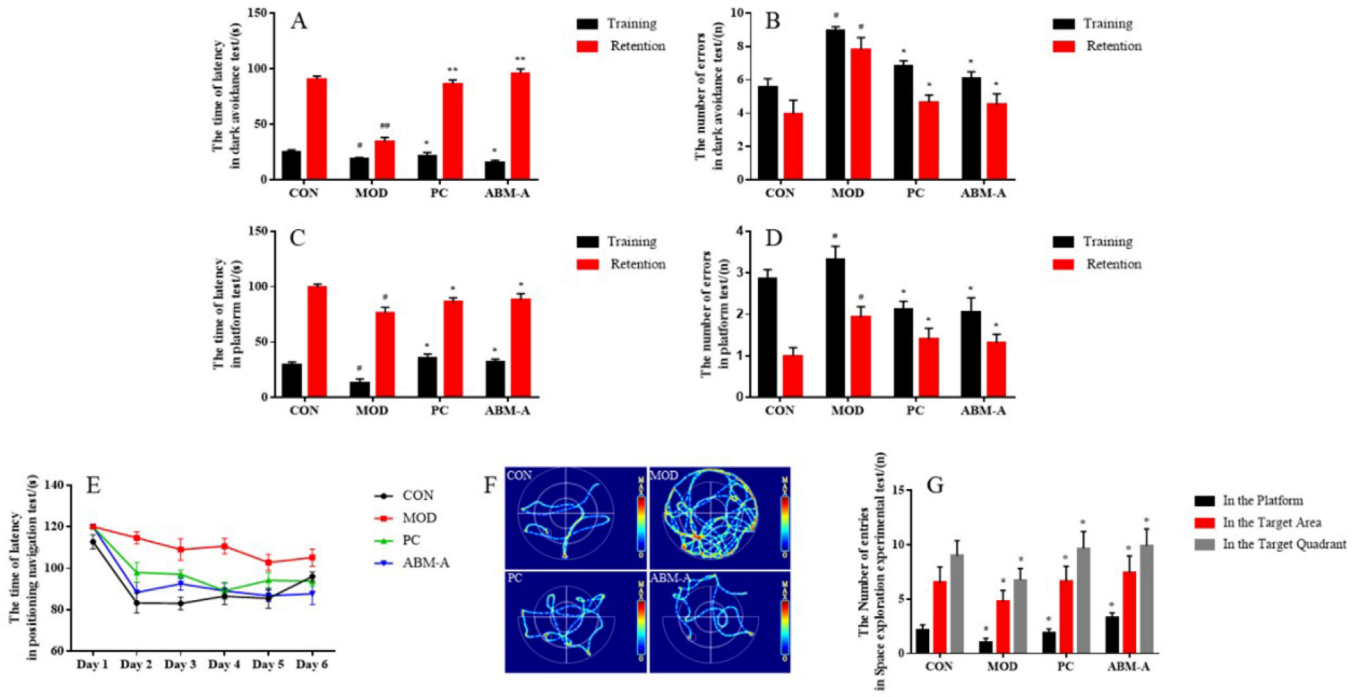

Fig. 2. Effects of AMB-A on the learning and memory of aging mice in behavioral experiments (Mean ± *SD*, n = 18). Step-through test: A: latency; B: number of errors. Step-down test: C: latency; D: number of errors. Morris water maze test: E: latency in orientation navigation test; F: analysis of the thermal map in orientation navigation test; G: spatial probe test. *: $p < 0.05$, **: $p < 0.01$, *vs* CON group; #: $p < 0.05$, ##: $p < 0.01$, *vs* MOD group.

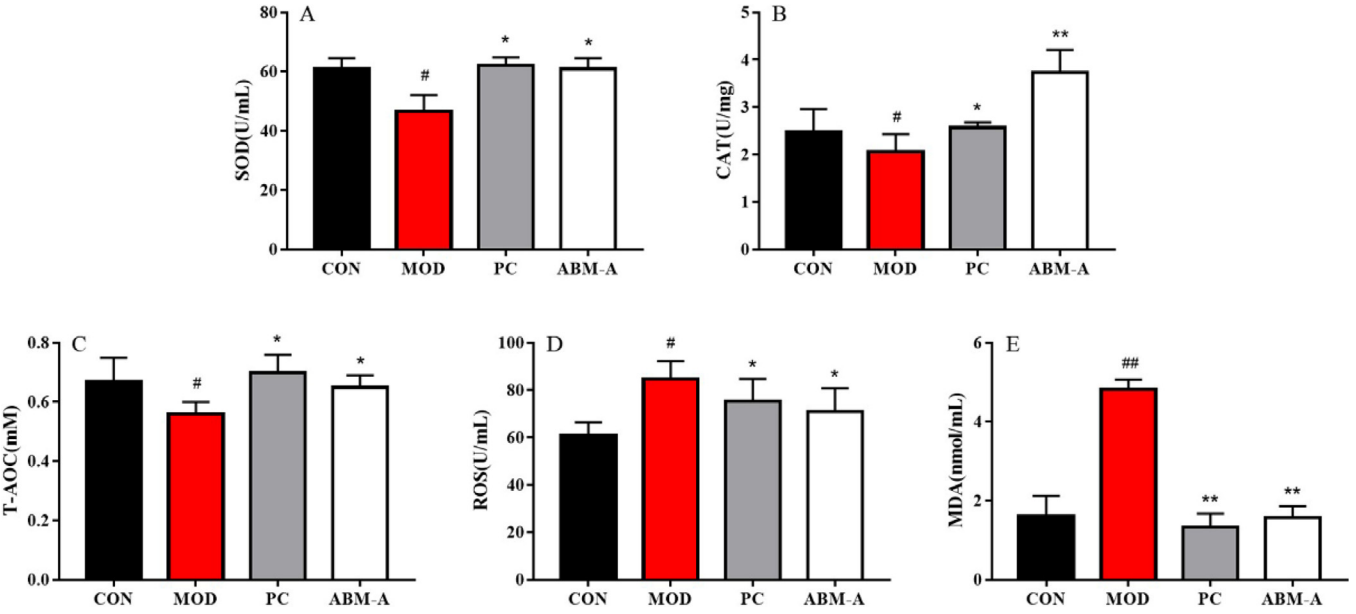

Fig. 3. Effects of ABM-A on serum biochemical indicators in D-gal-induced aging mice (Mean ± *SD*, n = 6). A: SOD activities; B: CAT activities; C: T-AOC contents; D: ROS contents; E: MDA contents. *: $p < 0.05$, **: $p < 0.01$, *vs* CON group; #: $p < 0.05$, ##: $p < 0.01$, *vs* MOD group.

cules (CAMs), Phagosome, Herpe simplex infection, Vials carcinogenesis, and HTLV-I inflection pathway, as shown in Fig. 5C.

Screening of differentially expressed genes: edgeR was used for the differential analysis of StringTie-assembled and quantified genes (the threshold of significant difference was |log2foldchange| $\geq$ 1, $p < 0.05$). Compared with MOD group, 168 differentially expressed genes were screened out, of which 101 of them were up-regulated genes and 67 down-regulated genes, in ABM-A group, as shown in Fig. 4D and E. According to the criteria of FPKM > 10, Pval < 0.05, FC > 1.5 and fc < 0.6, the differentially expressed genes were screened, and then according to the Gene ID and Transcript ID of the differentially expressed genes, the localization in the result table of protein annotation was performed to determine the protein and gene relationship network, and 18 differentially expressed

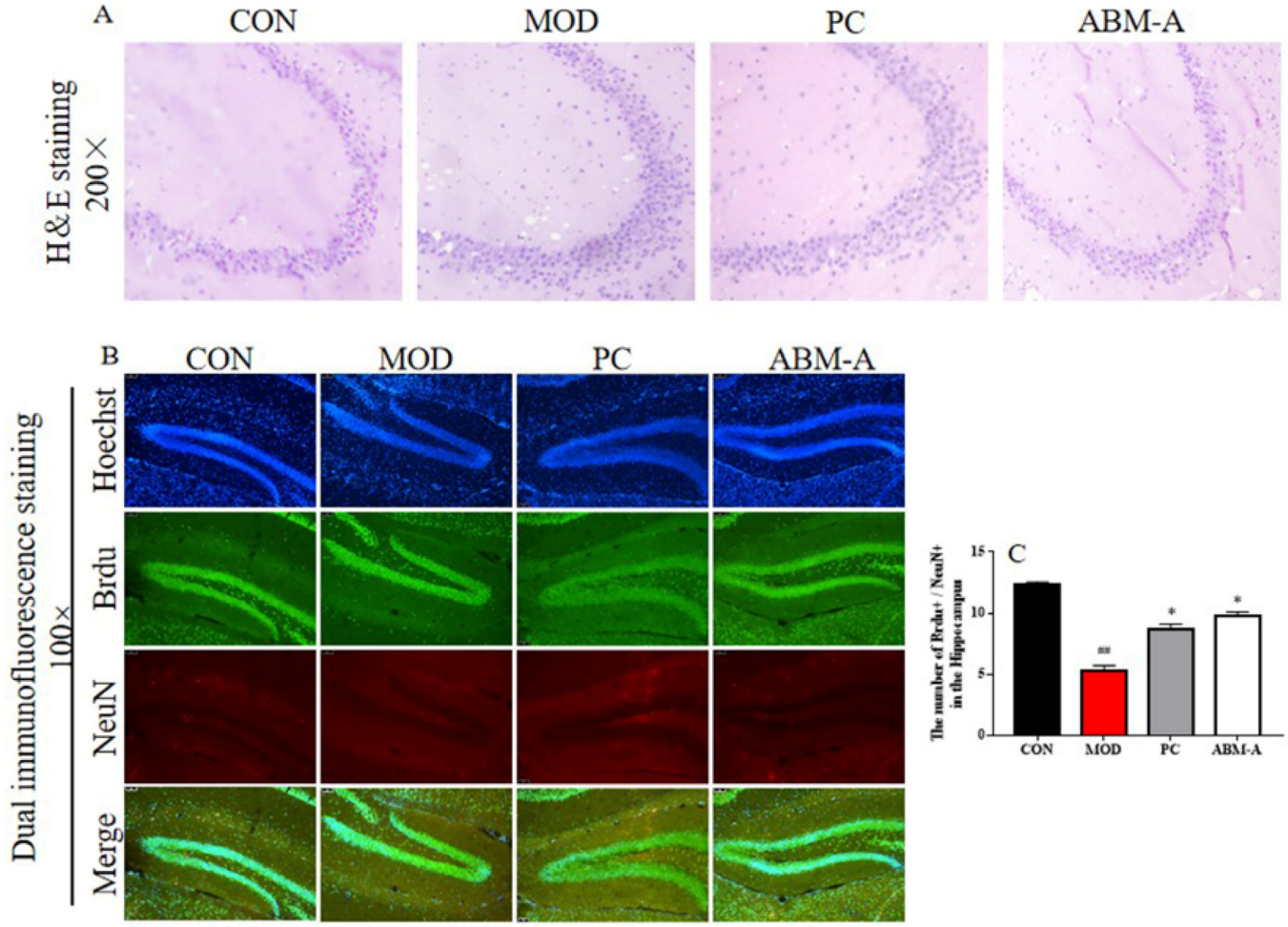

Fig. 4. Effects of ABM-A on pathological changes of the hippocampus of D-gal-induced aging mice. A: HE staining; B: immunofluorescence double labeling staining; C: Expression of BrdU/NeuN. *: $p < 0.05$, **: $p < 0.01$, *vs* CON group; #: $p < 0.05$, ##: $p < 0.01$, *vs* MOD group.

Table 4
Quality control and de novo assembly of RNA-Seq data.

Sample	Raw data		Valid Data		Valid Ratio(reads)	Q20%	Q30%	GC content%
	Read	Base	Read	Base				
ABM-A1	52971374	7.95G	52009586	7.80G	98.18	99.82	96.92	48.50
ABM-A2	46318466	6.95G	45348742	6.80G	97.91	99.79	97.54	49.50

genes Ank3, Apc, Apoe, Atp1a3, Atp6v0c, Atp6v1g2, Bmi1, Cox7a2l, Dpm3, Gabbr1, Hnrnpa1, Iqsec1, Plch2, Prkacb, Rpl24, Spcs1, Taok3 and Trim32 were obtained.

3.3.3. Effect of ABM-A on the expression of differentially expressed gene mRNA verified by qRT-PCR

In order to verify the accuracy and reliability of RNA-seq sequencing, nine differentially expressed genes, Cox7a2l, Taok3, Gabra1, Apoe, Ank3, Ndufv1, Atp1a3, Apc and Bmi1, were selected, and further verified by qRT-PCR. Using GAPDH as the internal reference gene, the amplification curve and dissolution curve of the genes met the requirements. Compared with those in MOD group, the expression levels of Cox7a2l, Ndufv1, Taok3, Gabra1 and Bmi1 in the hippocampal tissue of mice were significantly increased ($p < 0.05$), and those of Apoe and Atp1a3 were significantly decreased ($p < 0.05$) in ABM-A group. The results of RT-qPCR test were completely consistent with those of RNA-seq, demonstrating that the results of RNA-seq were reliable. Taking GAPDH as the internal reference and using 2^-△△Ct to plot, the relative expression levels of Cox7a2l, Taok3, Gabra1, Apoe, Ank3, Ndufv1, Atp1a3, Apc and Bmi1 genes in each sample were calculated (Fig. 6).

3.3.4. Effects of ABM-A on the expression of differential gene-related proteins verified by Western Blot

The results of Western Blot (Fig. 7) showed that compared with those in CON group, the expression levels of Nfe2l2, Hmox1, Myd88, p-c-Jun, Apc, Bmi1, Cox7a2l and Ndufv1 proteins were significantly decreased, those of Keap1, Apoe, Mapk1 and Atp1a3 proteins were significantly increased, and the phosphorylation levels of p38/p-p38 and Jnk/p-Jnk were significantly increased in the hippocampal tissue of aging mice in MOD group. Compared with those in MOD group, the expression levels of Keap1, Apoe, Mapk1 and Atp1a3 proteins were significantly decreased, and those of Nfe2l2, Hmox1, Myd88, p-c-Jun, Apc, Bmil, Cox7a2l and Ndufv1 proteins were significantly increased in the hippocampal tissue of mice in PC and ABM-A group. The results of Western Blot were consistent

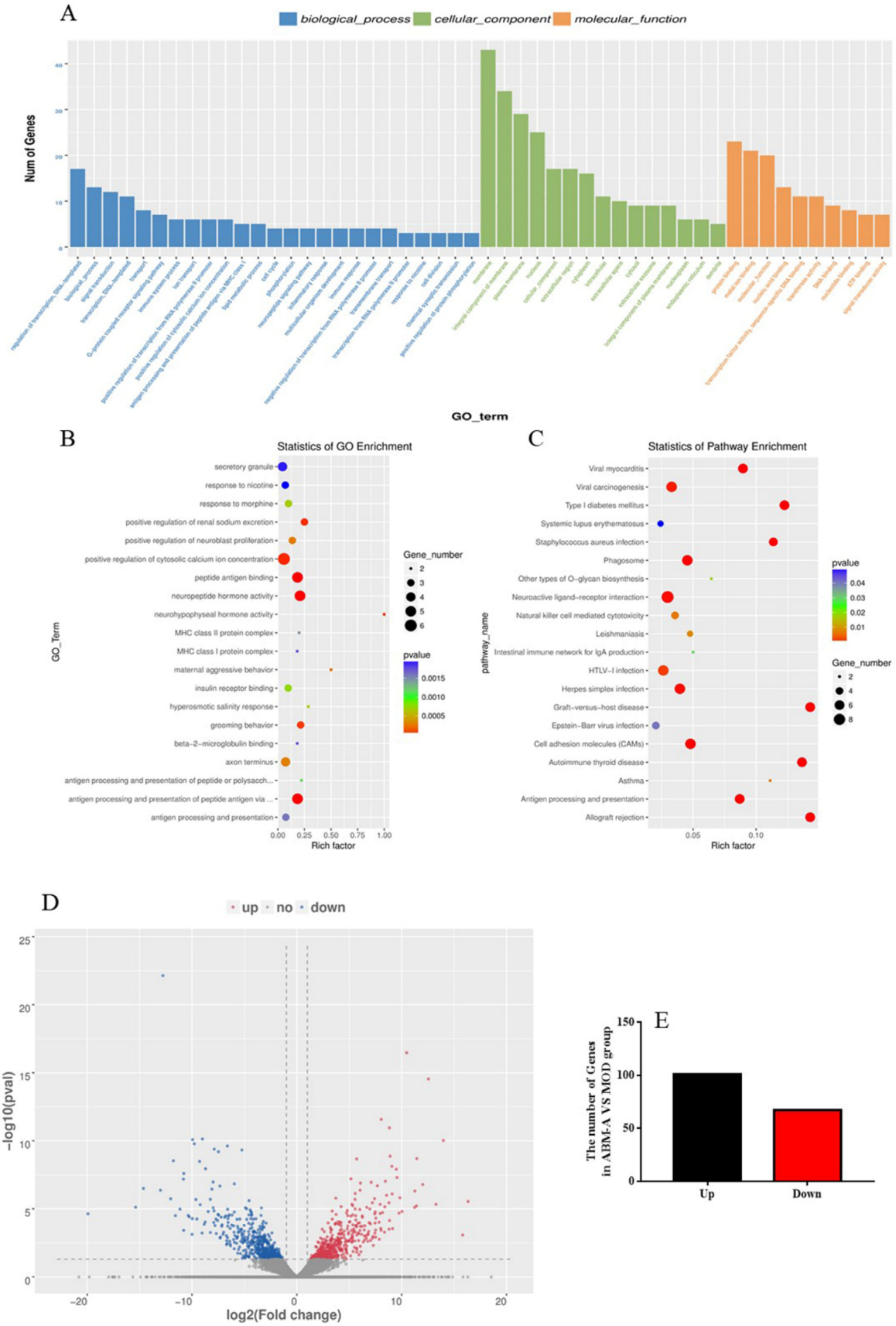

Fig. 5. Sequencing of transcriptome. A: GO functional classification; B: GO enrichment analysis, Rich factor denotes the number of differentially expressed genes located in the GO/the total number of genes located in the GO, and the greater Rich factor, the higher the GO enrichment degree; C: KEGG pathway analysis, RichFactor denotes the number of differentially expressed genes located in the KEGG/the total number of genes located in the KEGG, and the greater the RichFactor value, the greater the KEGG enrichment degree; D: Statistical volcano plot of differentially expressed genes between ABM-A and MOD groups; E: Statistical quantitative bar chart of differentially expressed genes between ABM-A and MOD groups.

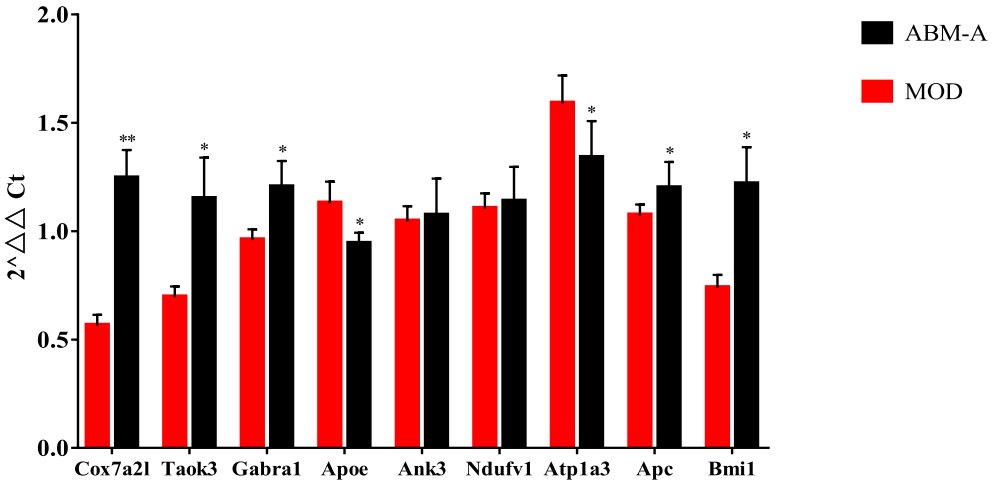

Fig. 6. Relative expression levels of differentially expressed genes. #: $p < 0.05$, ##: $p < 0.01$, *vs* MOD group.

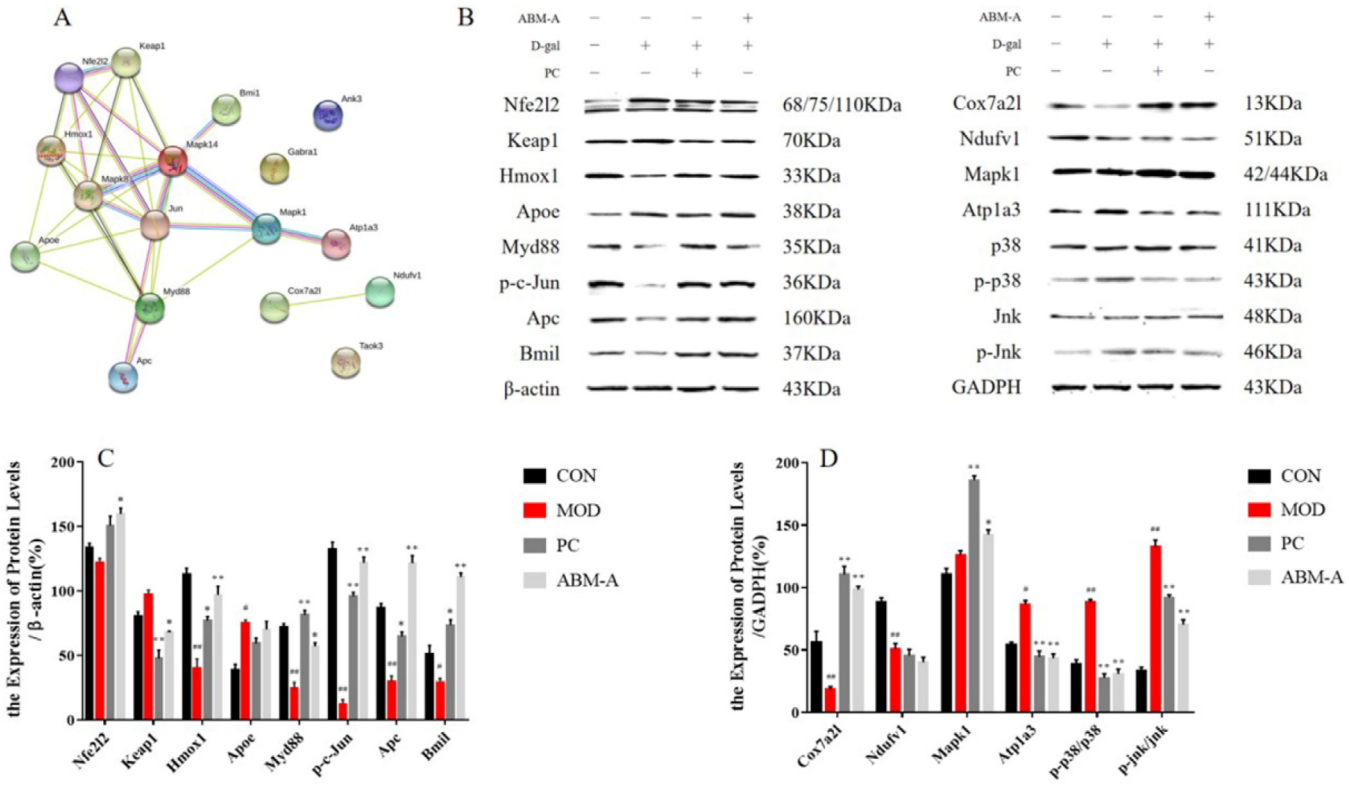

Fig. 7. Expression of differentially expressed genes and related proteins verified By Western Blot. A: STRING protein–protein network diagram of differential gene-related proteins; B: Western Blot results; C and D: Western Blot quantitative results. *: $p < 0.05$, **: $p < 0.01$, *vs* CON group; #: $p < 0.05$, ##: $p < 0.01$, *vs* MOD group.

with those detected by qRT-PCR, further verifying that the regulatory effect of ABM-A should be related to the up-regulated expression of Hmox1, Myd88, p-c-Jun, Apc, Bmil, Cox7a2l and Ndufv1, the down-regulated expression ofNfe2l2, Keap1, Apoe, Mapk1 and Atp1a3, and the decreased phosphorylationin of p38 and Jnk in D-gal-induced aging mice.

4. Discussion

Aging is the last stage of life, a process in which various functions of the body decline over time, which is closely related to the accumulation of ROS and oxidative stress [15]. Oxidative stress induced by excessive ROS can adversely affect the body, leading to the occurrence of age-related pathological diseases. D-gal, as a physiological nutrient, is normally metabolized into glucose and participates in the metabolism of glucose in the body, but excessive D-gal cannot be metabolized and accumulate in cells, producing a large number of reactive oxygen species such as O^{-2} and OH, which can also affect the synthesis of proteins including antioxidant enzymes due to metabolic disorders and the ability of scavenging free radicals to result in the production of excessive ROS, inducing oxidative stress in which the increased lipid peroxidation can damage cell membrane to cause metabolic disorders and cognitive impairment [16]. Therefore, the oxidative damage, inflammation and apoptosis caused by excessive D-gal are similar to

the symptoms of natural aging, and D-gal can be given to rodents in a long term to establish a good model for the study on the anti-aging effect of drugs [17]. In this study, after the continuous administration of excessive D-gal, the activity of mice decreased, the hair of mice fell off and the latency was prolonged in the navigation test, and the latency was shortened and the number of errors was increased in the step-through test and step-down test in MOD group, indicating that the long-term continuous injection of high-dose D-gal would seriously damage the spatial learning and memory ability of mice, and the aging model of mice was successfully established. After the administration of ABM-A, the general state and the learning and memory ability of mice were significantly improved, suggesting that ABM-A could improve the impaired learning and memory caused by aging. The detection of biochemical indicators showed that compared with those in MOD group, the SOD and CAT activities, and T-AOC levels increased, the MDA and ROS contents decreased in the serum of mice in ABM-A group, indicated that ABM-A could inhibit the continuous damage induced by H_2O_2 to slow down the oxidative damage induced by D-gal, showing a good protective effect in the aging mice.

Hippocampus is one of the most important brain regions to regulate stress response, and it is also one of the most vulnerable regions of nerve injury. The number of neurons in hippocampus decreases with ageing [18,19]. The pathological examination showed that the hippocampus of mice was damaged and the number of neurons decreased in MOD group, and the treatment of ABM-A could significantly improve the pathological changes induced by the excessive D-gal and increase the number of surviving neurons in the hippocampus of mice. It can be seen that the ABM-A can be used as an antioxidant to reduce the production of lipid peroxides in the oxidative stress induced by excessive D-gal to improve the damage of the hippocampal tissue, with an anti-aging effect.

As one of the important signaling pathways in oxidative stress, Keap1-Nrf2/ARE is the main pathway for preventing the damage caused by exogenous substances and cell oxidation, reducing the oxidative stress and mediating the antioxidant activity of the body [20,21]. Transcription factor Nrf2 is at the central position of oxidative stress and exists in the cytoplasm, and the activated Nrf2 after oxidation is separated from its negative regulatory factor Keapl and transferred into the nucleus under the action of multiple phosphorylation of ERK-mediated p38 and p-Jnk to bind to the cis-acting element ARE (antioxidant response element) on DNA to up-regulate the transcription and expression of downstream gene HO-1 [22]. The expression of Keap1 was down-regulated, and the expression of Nrf2 and HO-1 was up-regulated after the administration of ABM-A, indicating that the anti-aging effect of ABM-A could be related to the activation of Keap1-Nrf2/ARE pathway. MAPK is a central pathway involved in the Nrf2 activation and translocation for the synthesis of highly specialized proteins, including most readily inducible HO-1.MAPKs superfamily consists of three subfamilies: ERK1/2, JNK/SAPK, and p38 MAPK, of which ERK1/2 signaling pathway is mainly responsible for the transduction of cell growth, division and differentiation signals, while JNK/SAPK and p38 MAPK signaling pathways are mainly responsible for the transduction of inflammatory cytokines and various types of cell stress signals [23,24]. According to the STRING protein–protein relationship network, differential genes Apoe, Atp1a3, Apc and Bmi1 are closely related to MAPKs signal transduction pathway-related factors Mapk1, p38 and Jnk, of which Apoe is a polymorphic protein involved in the transformation and metabolism of lipoproteins, and its gene can regulate multiple biological functions and neuron injury to increase the level of Apoe in the brain [25]; the presence of Apoe4 allele reduces the neuronal repair ability of AD patients, and it has been reported that Apoe4 is related to spatial learning and memory impairment [26]. Atp1a3 gene encodes the α 3 subunit of Na^+/K^+-ATPase pump expressed in neurons, causing alternating hemiplegia in childhood, and the mutation of Atp1a3 can lead to the attack of acute neurode compensation in childhood [27]. Apc, as the key negative regulator of Wnt pathway to connect the framework of β-catenin degradation complex composed of Apc, glycogen synthase kinase-3P and axi, plays an important role by regulating the cell cycle and affecting the movement and adhesion of cells [28]. Bmi1 plays a role in the self-renewal of stem cells, and the high expression of Bmi1 can promote the proliferation of intestinal cells, inhibit the expression of INK4a/ARF site, regulate p53 signal pathway and then regulate cell cycle and apoptosis [29]. The Western Blot detection further confirmed that the down-regulation of Apoe, Atp1a3 and ERK1/2, the up-regulation of Apc, Bmi1, Myd88 and p-c-Jun, and the decreased phosphorylation of p38 and Jnk after the administration of ABM-A, suggesting that the anti-aging effect of ABM-A may be related to the inhibition of MAPKs signal pathway, and the inhibition of MAPKs signaling pathway can further reduce the translocation of Nrf2 into the nucleus, thus enhancing the protective effect of ABM-A.

In addition, the data of transcriptome showed that the expression level of Taok3, Ank3, Gabra1, Cox7a2l and Ndufv1 increased after the administration of ABM-A, in which the protein encoded by Taok3 gene was serine-threonine protein kinase, which is the basic activity of activating p38/MAPK14 [30]. Ank3 is a member of encoding anchor protein family closely related to mental illness, and may be related to the development of nerve cells induced by anchor protein [31]. Gabra1 gene encodes gamma-aminobutyric acid (GABA) receptors, GABA is the main inhibitory neurotransmitter in mammal brain, and the mutation of Gabra1 can lead to seizures in childhood and adolescence, which is related to central nervous system diseases [32]. Cox7a2l, an IV Cox7a2 subunit-like protein of the mitochondrial respiratory chain complex, can change the metabolic characteristics of cells by affecting the assembly of supercomplex [33]. Ndufv1 is the subunit encoding NADH oxidoreducase (complex I) enzyme and the first enzyme complex in the electron transport chain of mitochondria, and its defects are related to encephalopathy and neurodegenerative diseases [34,35], indicating that the anti-aging effect of ABM-A may be related to the regulation of mitochondrial function, the improvement of lipoprotein metabolism and the promotion of neonatal neuron activities.

5. Conclusions

Agaricus blazei Murrill acidic polysaccharide (ABM-A) can improve the brain damage induced by D-gal, increase the activity of antioxidant enzymes, reduce the peroxidation of lipids, with an obvious anti-aging effect. ABM-A may play a role by activating Keap1-Nrf2/ARE and inhibiting MapKs superfamily signal pathway. This study may provide a theoretical guidance for the application of ABM-A as a raw material for food, medicine and health care products, and lay a foundation for its deep development.

Ethical approval

This study was performed according to the international, national and institutional rules considering animal experiments, clinical studies and biodiversity rights. This study was approved by the Ethics Committee of School of Basic Medical Sciences, Jilin University and each mouse was consented in a written informed consent form.

Financial support

This work was supported by project "2018C046-3" supported by Development and Reform Commission of Jilin Province, project "201731201" supported by Science and Technology Bureau of Jilin City, project "2019Q020" supported by Jilin Department of Health, project "31900918" supported by National Natural Science Foundation of China, and project "2019128" supported by Jilin Provincial Administration of Traditional Chinese Medicine, and National and Local United Engineering Research and Development Center for research on active peptides of medicinal plants and animals in Changbai Mountains.

Conflict of interest

The authors declare no competing interest.

References

[1] Bishop NA, Lu T, Yankner BA. Neural mechanisms of ageing and cognitive decline. Nature 2010;464(7288):529–35. https://doi.org/10.1038/nature08983. PMid: 20336135.
[2] Di Micco R. Sensing the breaks: cytosolic chromatin in senescence and cancer. Trends Mol Med 2017;23(12):1067–70. https://doi.org/10.1016/j.molmed.2017.10.009. PMid: 29133134.
[3] Zhang ZF, Fan SH, Zheng YL, et al. Purple sweet potato color attenuates oxidative stress and inflammatory response induced by D-galactose in mouse liver. Food Chem Toxicol 2009;47(2):496–501. https://doi.org/10.1016/j.fct.2008.12.005. PMid: 19114082.
[4] Sfeir AJ, Chai W, Shay JW, et al. Telomere-end processing: the terminal nucleotides of human chromosomes. Mol Cell 2005;18(1):131–8. https://doi.org/10.1016/j.molcel.2005.02.035. PMid: 15808515.
[5] Xian YF, Su ZR, Chen JN, et al. Isorhynchophylline improves learning and memory impairments induced by D-galactose in mice. Neurochem Int 2014;76:42–9. https://doi.org/10.1016/j.neuint.2014.06.011. PMid: 24984171.
[6] Khan MZ, Atlas N, Nawaz W. Neuroprotective effects of *Caralluma tuberculata* on ameliorating cognitive impairment in a d-galactose-induced mouse model. Biomed Pharmacother 2016;84:387–94. https://doi.org/10.1016/j.biopha.2016.09.055. PMid: 27668539.
[7] Walker CL, Pomatto LCD, Tripathi DN, et al. Redox regulation of homeostasis and proteostasis in peroxisomes. Physiol Rev 2018;98(1):89–115. https://doi.org/10.1152/physrev.00033.2016. PMid: 29167332.
[8] Liu ZQ. Bridging free radical chemistry with drug discovery: A promising way for finding novel drugs efficiently. Eur J Med Chem 2020;189:. https://doi.org/10.1016/j.ejmech.2019.112020. PMid: 32006794112020.
[9] Kolsi RBA, Gargouri B, Sassi S, et al. *In vitro* biological properties and health benefits of a novel sulfated polysaccharide isolated from *Cymodocea nodosa*. Lipids Health Dis 2017;16(1):56–9. https://doi.org/10.1186/s12944-017-0643-v. PMid: 29273029.
[10] Wu S, Li F, Jia S, et al. Drying effects on the antioxidant properties of polysaccharides obtained from *Agaricus blazei Murrill*. Carbohydr Polym 2014;103(15):414–7. https://doi.org/10.1016/j.carbpol.2013.11.075. PMid: 24528748.
[11] Lin MH, Lee KM, Hsu CY, et al. Immunopathological effects of *Agaricus blazei* Murill polysaccharides against *Schistosoma mansoni* infection by Th1 and NK1 cells differentiation. Int Immunopharmacol 2019;73:502–14. https://doi.org/10.1016/j.intimp.2019.05.045. PMid: 31173972.
[12] Liu Y, Zhang L, Zhu X, et al. Polysaccharide *Agaricus blazei* Murill stimulates myeloid derived suppressor cell differentiation from M2 to M1 type, which mediates inhibition of tumour immune-evasion via the Toll-like receptor 2 pathway. Immunology 2015;146(3):379–91. https://doi.org/10.1111/imm.12508. PMid: 26194418.
[13] Wang W, Li P, Xu J, et al. Resveratrol attenuates high glucose-induced nucleus pulposus cell apoptosis and senescence through activating the ROS-mediated PI3K/Akt pathway. Biosci Rep 2017;38(2):. https://doi.org/10.1042/BSR20171454. PMid: 29273676BSR20171454.
[14] Hirsch EC, Hunot S. Neuroinflammation in Parkinson's disease: a target for neuroprotection? Lancet Neurol 2009;8(3):82–97. https://doi.org/10.1016/S1474-4422(09)70062-6.
[15] Bernhard EJ, McKenna WG, Hamilton AD, et al. Inhibiting Ras prenylation increases the radiosensitivity of human tumor cell lines with activating mutations of ras oncogenes. Cancer Res 1998;58(8):1754–61. PMid: 9563495.
[16] Sadigh-Eteghad S, Majdi A, McCann SK, et al. D-galactose-induced brain ageing model: a systematic review and meta-analysis on cognitive outcomes and oxidative stress indices. PLoS ONE 2017;12(8):. https://doi.org/10.1371/journal.pone.0184122. PMid: 28854284e0184122.
[17] Islam MT. Oxidative stress and mitochondrial dysfunction-linked neurodegenerative disorders. Neurol Res 2017;39(1):73–82. https://doi.org/10.1080/01616412.2016.1251711. PMid: 27809706.
[18] Feng Y, Yu YH, Wang ST, et al. Chlorogenic acid protects d-galactose-induced liver and kidney injury via antioxidation and anti-inflammation effects in mice. Pharm Biol 2016;54(10):27–34. https://doi.org/10.3109/13880209.2015.1093510. PMid: 26810301.
[19] Córdova NI, Turk BN, Aly M. Focusing on what matters: modulation of the human hippocampus by relational attention. Hippocampus 2019;29(11):1025–37. https://doi.org/10.1002/hipo.23082. PMid: 30779473.
[20] Kubben N, Zhang W, Wang L, et al. Repression of the antioxidant NRF2 pathway in premature aging. Cell 2016;165(6):1361–74. https://doi.org/10.1016/j.cell.2016.05.017. PMid: 27259148.
[21] Mahmoud AM, Germoush MO, Alotaibi MF, et al. Possible involvement of Nrf2 and PPARγ up-regulation in the protective effect of umbelliferone against cyclophosphamide-induced hepatotoxicity. Biomed Pharmacother 2016;86:297–306. https://doi.org/10.1016/j.biopha.2016.12.047. PMid: 28011377.
[22] Yao P, Nussler A, Liu L, et al. Quercetin protects human hepatocytes from ethanol-derived oxidative stress by inducing heme oxygenase-1 via the MAPK/Nrf2 pathways. J Hepatol 2007;47(2):253–61. https://doi.org/10.1016/j.jhep.2007.02.008. PMid: 17433488.
[23] Kim EK, Choi EJ. Pathological roles of MAPK signaling pathways in human diseases. Biochim Biophys Acta 2010;1802(4):396–405. https://doi.org/10.1016/j.bbadis.2009.12.009. PMid: 20079433.
[24] Johnson GL, Lapadat R. Mitogen-activated protein kinase pathways mediated by ERK, JNK, and p38 protein kinases. Science 2002;298(5600):1911–2. https://doi.org/10.1126/science.1072682. PMid: 12471242.
[25] Sebastiani P, Monti S, Morris M, et al. A serum protein signature of *APOE* genotypes in centenarians. Aging Cell 2019;18(6):. https://doi.org/10.1111/acel.13023. PMid: 31385390e13023.
[26] Smiderle FR, Sassaki GL, Van Griensven LJLD, et al. Isolation and chemical characterization of a glucogalactomannan of the medicinal mushroom *Cordyceps militaris*. Carbohydr Polym 2013;97(1):74–80. https://doi.org/10.1016/j.carbpol.2013.04.049. PMid: 23769519.
[27] Van Veen S, Sørensen DM, Holemans T, et al. Cellular function and pathological role of ATP13A2 and related P-type transport ATPases in Parkinson's disease and other neurological disorders. Front Mol Neurosci 2014;7:48. https://doi.org/10.3389/fnmol.2014.00048. PMid: 24904274.
[28] Tejeda-Muñoz N, Albrecht LV, Bui MH, et al. Wnt canonical pathway activates macropinocytosis and lysosomal degradation of extracellular proteins. Proc Natl Acad Sci USA 2019;116(21):10402–11. https://doi.org/10.1073/pnas.1903506116. PMid: 31061124.
[29] Flamier A, El Hajjar J, Adjaye J, et al. Modeling late-onset sporadic Alzheimer's disease through BMI1 deficiency. Cell Rep 2018;23(9):2653–66. https://doi.org/10.1016/j.celrep.2018.04.097. PMid: 29847796.
[30] Gu X, Zhou Y, Hu X, et al. Reduced numbers of cortical GABA-immunoreactive neurons in the chronic D-galactose treatment model of brain aging. Neurosci Lett 2013;549:82–6. https://doi.org/10.1016/j.neulet.2013.06.021. PMid: 23806602.
[31] Zhang C, Cai J, Zhang J, et al. Genetic modulation of working memory deficits by ankyrin 3 gene in schizophrenia. Prog Neuropsychopharmacol Biol Psychiatry 2014;50:110–5. https://doi.org/10.1016/j.pnpbp.2013.12.010. PMid: 24361380.
[32] Hoftman GD, Volk DW, Bazmi HH, et al. Altered cortical expression of GABA-related genes in schizophrenia: illness progression vs developmental disturbance. Schizophr Bull 2015;41(1):180–91. https://doi.org/10.1093/schbul/sbt178. PMid: 24361861.
[33] Lobo-Jarne T, Nývltová E, Pérez-Pérez R, et al. Human COX7A2L regulates complex III biogenesis and promotes supercomplex organization remodeling without affecting mitochondrial bioenergetics. Cell Rep 2018;25(7):1786–1799.e4. https://doi.org/10.1016/j.celrep.2018.10.058. PMid: 30428348.
[34] Kapfhamer D, King I, Zou ME, et al. JNK pathway activation is controlled by Tao/TAOK3 to modulate ethanol sensitivity. PLoS ONE 2012;7(12):. https://doi.org/10.1371/journal.pone.0050594. PMid: 23227189e50594.
[35] Wadhwa Y, Rohilla S, Kaushik JS. Cystic leucoencephalopathy in *NDUFV1* mutation. Indian J Pediatr 2018;85(12):1128–31. https://doi.org/10.1007/s12098-018-2721-1. PMid: 29948731.